NAR Molecular Medicine, 2024, **1**, ugae021
https://doi.org/10.1093/narmme/ugae021
Advance access publication date: 23 November 2024
Standard Article

Conformation-specific RNA aptamers for phenotypic distinction between normal von Willebrand factor and type 2B von Willebrand disease

Venkata R. Machha[1,2], Alexander Tischer[1,2], Laurie Moon-Tasson[1], Julie Tange[3], Annyoceli Santiago-Davis[2], Rajiv K. Pruthi[4], Dong Chen[5], L. James Maher, III[2] and Matthew Auton[1,2,*]

[1]Division of Hematology, Department of Internal Medicine, Mayo Clinic, 200 1st St SW, Rochester, MN, USA
[2]Department of Biochemistry and Molecular Biology, Mayo Clinic, 200 1st St SW, Rochester, MN 55905, USA
[3]Special Coagulation Laboratory, Mayo Medical Laboratories, Mayo Clinic, 200 1st St SW, Rochester, MN 55905, USA
[4]Division of Hematopathology, Division of Laboratory Genetics and Genomics, Department of Laboratory Medicine and Pathology, Mayo Clinic, 200 1st St SW, Rochester, MN 55905, USA
[5]Division of Hematopathology, Department of Laboratory Medicine and Pathology, Mayo Clinic, 200 1st St SW, Rochester, MN 55905, USA
[*]To whom correspondence is addressed. Tel: +1 507 284 3776; Email: auton.matthew@mayo.edu

Abstract

The A1 domain in Von Willebrand Factor (VWF) initiates coagulation through binding to platelet glycoprotein GPIbα receptors. Von Willebrand Disease (VWD)-Mutations in A1 that either impair (type 2M) or enhance (type 2B) platelet adhesion to VWF can locally destabilize and even misfold the domain. We leveraged misfolding in the gain-of-function type 2B VWD phenotype as a target, distinct from the normal conformation. Two nuclease-resistant 2′-fluoropyrimidine RNA aptamers were selected to discriminate normal A1 domains from a type 2B V1314D A1 variant in a glycosylated A1A2A3 tri-domain VWF-fragment. Two aptamers, W9 and V1, were isolated that selectively recognize, bind, and inhibit the A1–GPIbα interaction with WT A1A2A3 and V1314D A1A2A3, respectively. These aptamers were tested against their respective recombinant targets, plasma VWF, VWF concentrates, and patient plasma with the heterozygous type 2B VWD R1306W variant using clinical assays, surface plasmon resonance and inhibition assays of platelet adhesion to recombinant A1 and A1A2A3 domains under shear stress. The specificity of W9 and V1 aptamers confirms that pathological conformations of VWD Type 2B proteins are different from normal VWF. The availability of aptamers that distinguish normal plasma-derived VWF from VWD suggests potential applicability in clinical diagnosis of severe gain-of-function phenotypes.

Graphical abstract

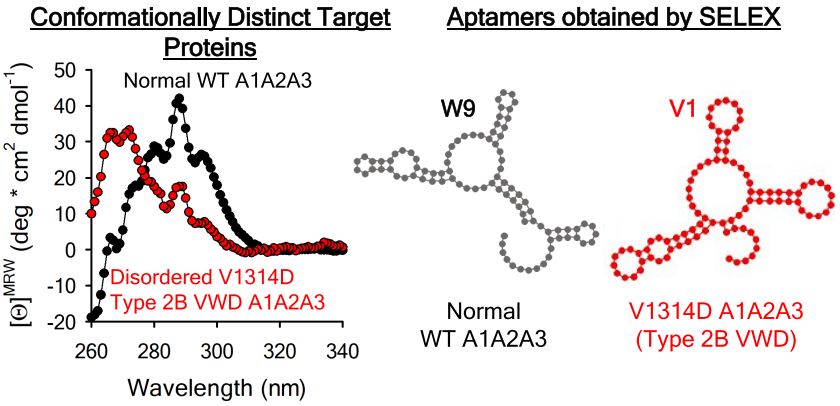

Introduction

The primary hemostatic function of the plasma protein von Willebrand factor (VWF) is to capture and deposit platelets at damaged subendothelial sites of cardiovascular injury. VWF is secreted from endothelial cells as a long multimer of dimers and becomes activated in response to the elevated shear stress

Received: October 10, 2024. **Revised:** November 14, 2024. **Editorial Decision:** November 19, 2024. **Accepted:** November 22, 2024

of blood flow that exposes the GPIbα binding A1 domains of VWF multimers (1). VWF also is a carrier for the hemophilia A related factor VIII (2).

Von Willebrand disease (VWD) comprises a large number of genetic mutations resulting in amino acid substitutions that are classified into three major subtypes (3–5). Types 1 and 3 VWD introduce a quantitative VWF deficiency that causes reduced VWF plasma levels. Type 3 is a more severe quantitative deficiency than type 1. Type 2 VWD introduces qualitative defects within the A1 and A2 domains that alter A1 affinity for platelet GPIbα (type 2B and 2M) and cause the A2 domain to be more susceptible to ADAMTS13 proteolysis (type 2A) resulting in a quantitative reduction of high molecular weight multimers, respectively (6,7). Both function defects, i.e. gain-of-function (type 2B, sometimes associated with reduced high molecular weight multimers) and loss-of-function (type 2M, normal multimers), result in prolonged bleeding and primary hemostatic complications (8,9). Although type 2 VWD is a rare bleeding disorder, anti-VWF inhibitors, nanobodies and aptamers have been the subject of investigation as diagnostics and therapeutics over the last few decades.

The AU/VWFa-11 nanobody, obtained by llama immunization against high molecular weight multimers of normal VWF, has been used to detect type 2B VWD (10–12) with variable results. The bivalent humanized ALX-0681 nanobody obtained by llama immunization against the wild-type (WT) A1 domain (13) has achieved FDA approval (caplacizumab) for the treatment of thrombotic thrombocytopenic purpura (TTP) (14,15).

RNA and DNA aptamers have also been developed to bind and inhibit A1. Recently, rondaptivon pegol (16), also known as Rondoraptivon pegol (17) or BT200 (18–22), a polyethylene glycol-modified (PEGylated) and 2′-O-methyl ester derivatized RNA aptamer (BT100), has been shown to inhibit unusually large multimeric VWF-dependent platelet function (22), elevate plasma levels of VWF and factor VIII (21), increase platelet counts and VWF/FVIII in type 2B VWD (17), and inhibit VWF and FVIII clearance by blocking the interaction between A1 and the macrophage LRP1 receptor (19) through binding the K_{1405}-K_{1408} tetra-lysine sequence in the α4 helix of the A1 domain. This preparation has recently been used as a treatment for hemophilia A (16). BT100 is a derivative of ARC15105, to which four additional basepairs were added to stabilize a 5-base-pair stem-loop at physiological temperature (37°C). ARC15105 inhibited shear-induced platelet plug formation (23).

Another aptamer, ARC1779, has been recently demonstrated to improve the recovery, survival and function of refrigerated platelets (24). ARC1779 is a 2′-O-methoxy DNA/RNA hybrid with a phosphorothioate linkage and an inverted deoxythymidine (25). Developed as an antithrombotic agent that inhibits platelet activation and thrombosis (26), ARC1779 has seen clinical trials for type 2B VWD (27,28), congenital TTP (29–32), acquired TTP (33) and *ex vivo* applications to acute myocardial infarction (34). However, its clinical diagnostic utility for type 2B VWD was limited because it bound to ristocetin (27) and its specificity in type 2B clinical trials was questionable because patients were not genotyped (28). ARC1779 has the same sequence as the ARC1172 DNA aptamer selected for, and co-crystallized in complex with, the WT A1 domain that binds residues P_{1418}-K_{1423} leading into the α5 helix of A1 (35). Other aptamers (36) have also been selected for anti-VWF platelet function (37) and anti-A1 domain platelet function (33). However, all the aptamers and nanobodies developed to date have targeted the normal WT A1 domain.

Our interest in VWD centers on understanding the fundamental structure/function properties of the A1 domain harboring type 2B and type 2M mutations that have been clinically identified in patients with VWD. Our studies have shown that many VWD variants of the A1 domain in both phenotype classifications introduce localized structural disorder that favor nonnative misfolded conformational states (38–42). Within each VWD subtype, 2B and 2M, the thermodynamic stability is altered and extreme cases of amino acid substitutions abrogate folding to the native tertiary structure resulting a loss of helical structure in different regions of the A1 domain. Gain- or loss-of-platelet binding depends on where structural disorder occurs (38). In type 2B, destabilization of A1 results in enhanced dynamics in and around the α2 helix and extreme cases locally unfold this region to a partially disordered state that enhances the strength of platelet adhesion to A1 (40,43). In type 2M, variant-induced local unfolding of α3 or structural disorder in the C-terminal half of the A1 domain prevents platelet adhesion (40,43). At the other extreme, type 2M is caused by global stabilization of the A1 domain by variants that constrain the conformational dynamics of A1 so tightly that A1 is unable to adapt to the shear flow of blood resulting in unstable transient platelet attachment (44).

Given that the majority of type 2 VWD variants we previously studied were non-native conformations, we leveraged this fundamental property to develop aptamers that distinguish normal from disordered states of A1 within an A1A2A3 glycosylated tri-domain fragment of VWF. Nuclease-resistant 2′-fluoropyrimidine RNA aptamers were selected against WT and V1314D; a particularly detrimental variant that replaces a buried valine residue in the β2 strand of the central β-sheet with a charged aspartic acid. V1314D substantially affects the tertiary structural contacts holding the α2 helical region together and local unfolding of α2 leads to high strength platelet adhesion under shear stress (40) resulting in severe thrombocytopenia (45). Here, we demonstrate that two aptamers, W9 (targeting WT A1A2A3) and V1 (targeting V1314D A1A2A3), distinguish the type 2B phenotype from normal both in the biophysical context and in a clinical diagnostic setting. The results presented here thus advance a potentially novel diagnostic paradigm for accurate VWD phenotyping that may also be useful in a therapeutic context.

Materials and methods

VWF A1, A2 and A3 single domain expression and purification

A1 (Gln_{1238}-Pro_{1471}), A2 (Gly_{1481}-Ser_{1671}) and A3 (Ser_{1671}-Gly_{1874}) were expressed in *Escherichia coli* M15 cells as fusion proteins containing an N-terminal 6× His-tag, isolated, refolded and purified using Ni^{2+}-NTA affinity chromatography as described previously (46–48). A1 was further purified via heparin affinity chromatography.

VWF A1A2A3 tridomain purification and quantification

WT and V1314D VWF A1A2A3 tridomain variants (amino acids Q_{1238}–G_{1874}) were expressed in HEK293 cell culture as fusion proteins containing a C-terminal 6× His-tag and pu-

rified using Ni^{2+}-NTA affinity chromatography as described previously (46). Protein quality was confirmed by RP-HPLC after purification. Before selection, all purified protein targets were quantified on a Shimadzu UV2101PC spectrophotometer using an extinction coefficient of 74 497 L/mol/cm calculated from their amino acid sequence.

Aptamer selection

Aptamers were selected and enriched from a single-stranded DNA library (LJM-430) that includes a sequence of 55 random nucleotides (N) flanked by two fixed sequences that serve as binding sequences for polymerase chain reaction (PCR) amplification and cloning. RNA was prepared by *in vitro* transcription using the DuraScribe T7 Transcription Kit (Epicentre, Madison, WI), which contains 2′-fluorinated pyrimidines (2′-F-CTP and 2′-F-UTP) that confer nuclease resistance to transcribed RNA. Systematic Evolution of Ligands by EXponential enrichment (SELEX) was performed in parallel using both WT and V1314D VWF tri-domain variants as binding targets for aptamers. The double-stranded DNA libraries of cycle 7 for WT VWF A1A2A3 and cycle 9 for V1314D VWF A1A2A3 were ligated into the pGEM-TEasy vector using a TA cloning kit (Promega). Cloned sequences were aligned using multiple sequence alignment tool MUSCLE (EMBL).

For details, please see the Supplementary Data.

Surface plasmon resonance

Binding of SELEX selected RNA aptamers to VWF tridomain variants (WT and V1314D A1A2A3), A2 and A3 were characterized using a Biacore T-100. RNA aptamers were biotinylated at the 3′-terminus using a Pierce RNA 3′-Biotinylation kit (Thermo Scientific). Approximately 500 RU of biotinylated RNA aptamers were captured on an active channel of a streptavidin-pretreated dextran sensor surface (SA chip) by injecting between 100 and 200 μg/ml concentration of RNA in 10 mM HEPES, pH 7.4 at flow rates of 5 μl/min. Identical amounts of biotinylated cytidine were added on the control channel to subtract the non-specific response of VWF protein variants binding to streptavidin surface from the specific response of protein–RNA binding. VWF protein variants were diluted in a 10 mM HEPES buffer, pH 7.4 to various concentrations ranging from 2.5 to100 nM. They were injected across the active and reference surfaces at a flow rate of 30 μl/min at 37°C for 200 s of association and 400 s of dissociation. The RNA aptamer surface was regenerated by injecting a pulse of 5 M NaCl for 180 s and 8 M GuHCl for 60 s. The regeneration conditions were determined by preliminary studies using NaCl and GuHCl at various concentrations. Each analyte concentration is injected twice to be confident of reproducibility. All surface plasmon resonance (SPR) responses were double referenced before analysis to remove non-specific interactions and baseline drifts. Kinetic constants were determined by fitting response curves globally or locally using 1:1 binding model provided by Biacore Evaluation Software 3.0.

Shear-dependent rheological assay

Parallel plate flow chamber studies were performed with Vena8 GCS biochips on a Zeiss Axio Observer A1 microscope equipped with a PCO.edge camera and operated by the Zen2012 Software. 20 μl of either 5 μM WT A1A2A3 or 5 μM V1314D A1A2A3 was immobilized overnight at 4°C via its C-terminal 6×His tag on Cu^{2+}-treated Vena8 Chips (Cellix, Dublin, Ireland). Following A1A2A3 immobilization, flow chambers were rinsed with Tris-buffered saline (TBS) and 20 μl of either 5 μM W9 aptamer, 5 μM V1 aptamer or 0.3 mM transfer-RNA (tRNA) was incubated on surface immobilized A1A2A3 tridomains at 4°C for 2 h. Flow chambers were placed at room temperature for 1 h prior to the experiment. At the microscope, citrated whole blood kept at 37°C was perfused over at a shear rate of 800 s^{-1} and after ∼4 min, TBS was perfused through the channel to remove red blood cells. Movies were recorded at 25 frames/s. Images were taken from the movies and platelets were counted using the MediaCybernetics ImagePro Premier software (v9.3). As a control, these experiments were also performed using 5 μM A1, A2 and A3 single domains immobilized by the N-terminal 6×His tag and 5 μM W9 aptamer to demonstrate A1 domain specificity of W9 under flow. The A2 and A3 domains do not bind platelets.

Ristocetin induced platelet agglutination assay

The effect of VWF RNA aptamers on platelet aggregation induced by ristocetin was determined on a PAP-8E platelet aggregation profiler aggregometer. Reconstituted washed platelets were further diluted to 125 μl with diluent (20 mM Tris, 150 mM NaCl, pH 7.4) and incubated 50 μl normal pooled plasma (NPP) with and without aptamers of different concentrations (5, 10 and 100 nM) for 5 min at 37°C. Subsequently, preincubated NPP samples with and without aptamers were added to 125 μl washed platelets in a test tube and platelet aggregation was induced by adding 0.5 mg/ml ristocetin under constant stirring (1000 rpm). In the case of type-2B plasma, 0.375 mg/ml ristocetin was added, sufficient to induce platelet aggregation for the gain-of-function phenotype. Platelet aggregation was measured according to change in light transmission and plotted as % light transmission as a function of time in s.

VWF latex activity assay

Plasma VWF activity in presence of RNA aptamers was measured on an ACL TOP coagulation analyzer using a HemosIL VWF Latex assay kit. NPP was prediluted 1 part plasma and 2 parts diluent (20 mM Tris, 150 mM NaCl, pH 7.4) as per the kit instructions. NPP (30 μl) was preincubated with aptamer at a final concentration of 200 nM for 5 min at 37°C. VWF activity latex reagent (150 μl) was added to aptamer treated plasma, and latex bead agglutination was measured at 405 nm as a decrease in light transmission. Similarly, amount of VWF antigen in plasma samples was also measured using VWF antigen latex kit.

Spectroscopy and calorimetry

Circular dichroism (CD), fluorescence and calorimetry measurements were performed as previously described and are explained in detail in the Supplementary Data (40,46).

Results

The V1314D substitution misfolds the A1 domain within the A1A2A3 tri-domain

Previously, we described how misfolding of the VWF A1 domain manifests phenotypically for several type 2B and 2M VWD genetic variants (40). Among the VWD variants we have characterized, V1314D is an extreme gain-of-function

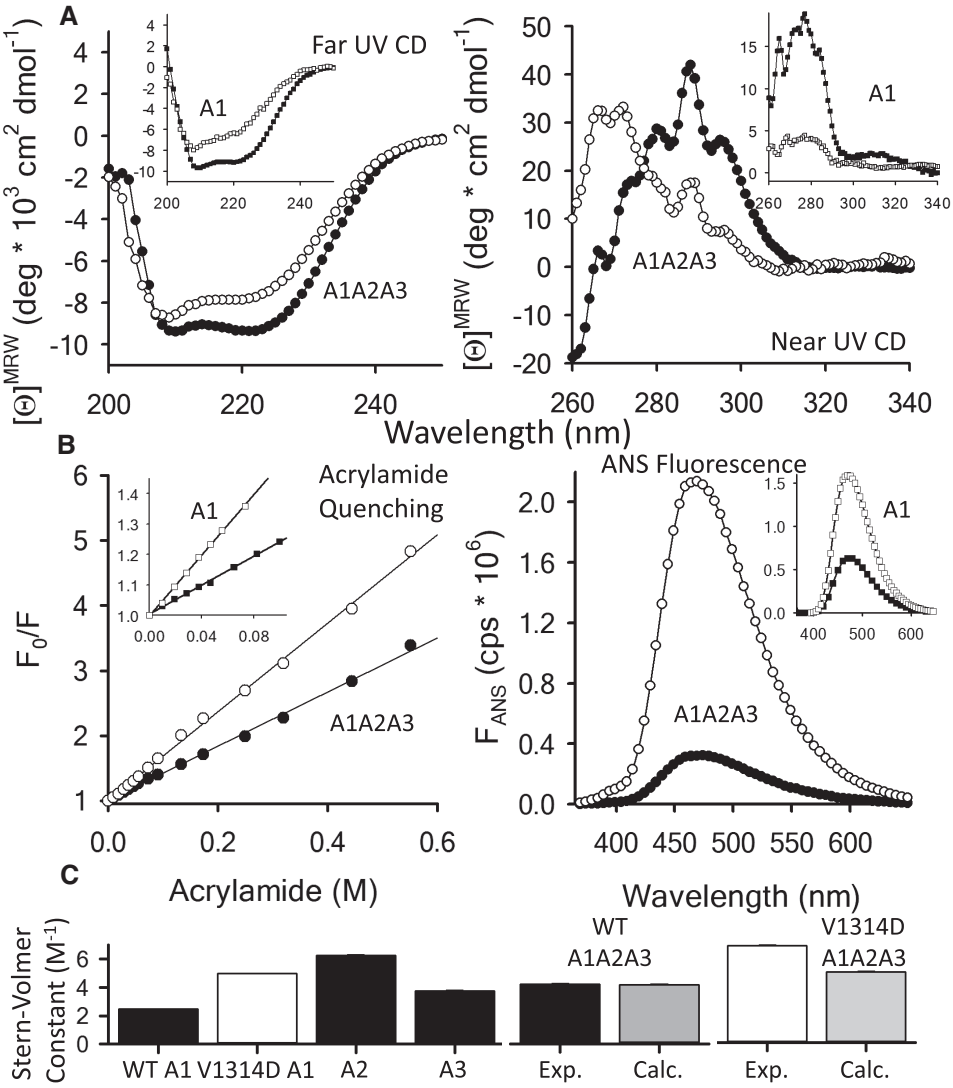

Figure 1. Spectroscopic characterization of WT A1A2A3 (●), V1314D A1A2A3 (○), WT A1 (■) and V1314D A1 (□). Panel (**A**) shows far- and near-UV CD spectra. (**B**) Quenching of fluorescence intensity with acrylamide at 20°C ($\lambda_{Excitation}$ = 295 nm and $\lambda_{Emission}$ = 359 nm) and spectra in presence of 100 μM ANS ($\lambda_{Excitation}$ = 350nm) at 20°C. Stern–Volmer constants, determined from the quenching experiments are plotted in panel (**C**). Acrylamide quenching experiments for WT A1, A2 and A3 can be found in the supplement. Experimental Stern–Volmer quenching constants, in units of L/mol, are 4.19 ± 0.04 for WT A1A2A3, 6.82 ± 0.06 for V1314D A1A2A3, 2.45 ± 0.03 for A1 (41), 4.96 ± 0.03 for V1314D A1, 6.26 ± 0.05 for A2 and 3.45 ± 0.03 for A3 (47). Calculated Stern–Volmer quenching constants from the average of the single domain quenching constants are 4.16 ± 0.04 for WT A1A2A3 and 4.99 ± 0.04 for V1314D A1A2A3. Note the agreement between experimental and calculated for WT A1A2A3, but not for V1314D A1A2A3. All A1A2A3 spectra were background corrected for the buffer (10 mM HEPES, pH 7.4, 150 mM NaCl, 1 mM EDTA). Insets represent identical data sets but with the single WT and V1314D A1 domains; data taken from reference (40).

variant with tight binding to platelets under shear flow, causing severe thrombocytopenia in type 2B VWD (40,45). V1314D replaces a hydrophobic valine in the hydrophobic core of A1 with a negatively charged aspartic acid. To obviate any misinterpretation that the misfolding of the A1 domain is due to heterologous bacterial expression, the V1314D variant was expressed in HEK293 cells within an A1A2A3 tri-domain fragment of VWF that includes the neighboring A2 and A3 domains and glycosylation sequences.

We previously demonstrated local unfolding and disorder of V1314D A1 within A1A2A3 using hydrogen deuterium exchange mass spectrometry (38). Here, we further demonstrate misfolding of A1 in A1A2A3 using the more common available spectroscopies. Figure 1A demonstrates that V1314D affects the overall secondary and tertiary structures of the A1A2A3 tri-domain. CD spectra obtained in the far-UV range indicate V1314D induces a loss of α-helical structure in both A1 and A1A2A3.

The CD spectra obtained in the near-UV range indicate that V1314D alters the tertiary structure fingerprint of both A1 and A1A2A3 due to an altered local environment affecting tryptophan and tyrosine residues. This is also evident from the increased acrylamide quenching of intrinsic tryptophan fluorescence by V1314D in both A1 and A1A2A3 (Figure 1B).

Provided that acrylamide quenching follows a dynamic collisional mechanism wherein excited tryptophan fluorophores are deactivated by transient interactions with acrylamide in solution, a larger slope (Stern–Volmer constant) indicates greater solvent accessibility of tryptophan. Figure 1C reports the quenching constants for the individual WT A1, V1314D

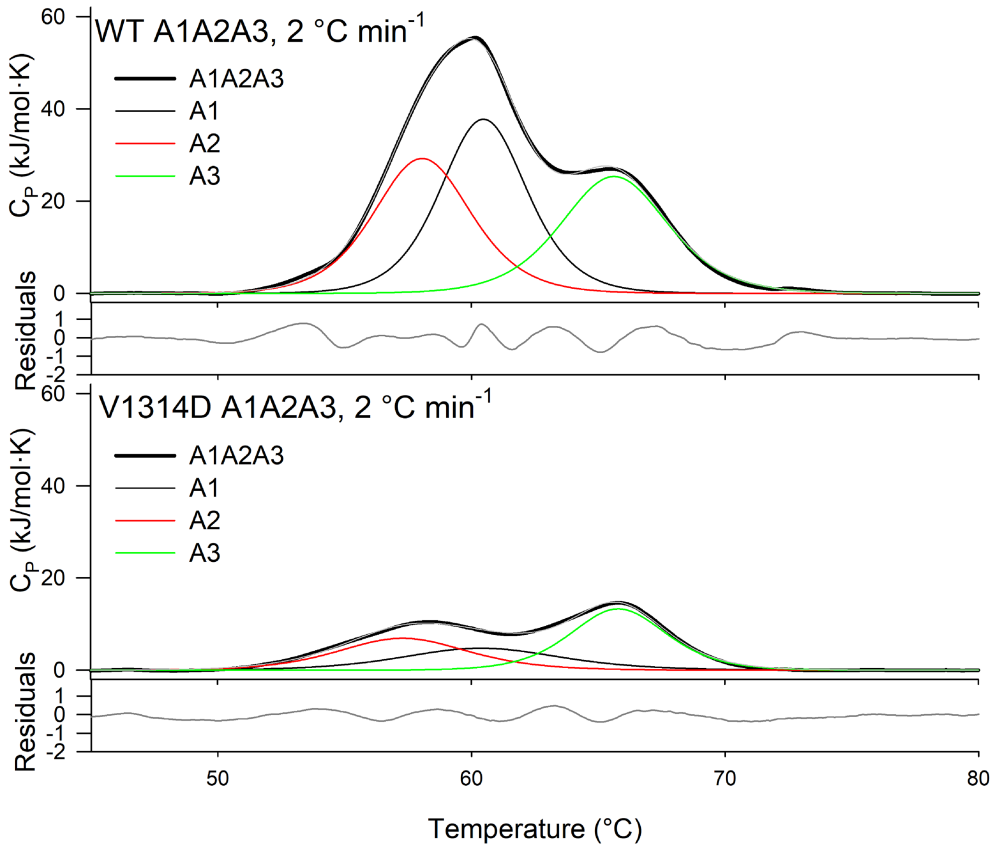

Figure 2. Thermal unfolding of WT (top) and V1314D A1A2A3 (bottom) measured by DSC at a scan rate of 2.0°C/min. Heat capacity thermograms were background corrected relative to the buffer (10 mM HEPES, pH 7.4, 150 mM NaCl, 1 mM EDTA) and normalized to a polynomial baseline to define the excess heat capacity. Excess heat capacity was fit using nonlinear least squares analysis and deconvoluted into individual A1, A2 and A3 domain contributions using Wolfram Mathematica per a thermodynamic model in which each domain thermally denatures in a two-state manner. Both panels contain deconvoluted thermograms of the single domains within the tri-domain. Fit residuals are shown at the bottom. Apparent thermal transition temperatures of the deconvoluted domains at a 2.0°C/min. A1: 60.49 ± 0.005°C in A1A2A3 versus 60.68 ± 0.03°C in V1314D A1A2A3. A2: 58.08 ± 0.005°C in A1A2A3 versus 57.27 ± 0.02°C in V1314D A1A2A3. A3: 65.65 ± 0.004°C in A1A2A3 versus 65.86 ± 0.005°C in V1314D A1A2A3. Apparent thermal transition enthalpies of the deconvoluted domains at a 2.0°C/min. A1: 171.6 ± 0.4 kJ/mol in A1A2A3 versus 40.8 ± 0.3 kJ/mol in V1314D A1A2A3. A2: 149.9 ± 0.4 kJ/mol in A1A2A3 versus 49.0 ± 0.3 kJ/mol in V1314D A1A2A3. A3: 142.7 ± 0.4 kJ/mol in A1A2A3 versus 67.2 ± 0.3 kJ/mol in V1314D A1A2A3.

A1, A2 and A3 domains and those of WT and V1314D A1A2A3 tridomains. Each of the domains contain a single tryptophan. The calculated average of the WT single domain quenching constants matches that of the experimentally determined WT A1A2A3 tridomain quenching constant indicating that the tryptophans are similarly exposed in the tridomain as they are in the single domains. By contrast, the calculated quenching constant for V1314D A1A2A3 is lower than what was determined experimentally. This discrepancy may be attributed to V1314D induced misfolding of A1 and potential changes to the quaternary structure of the A1A2A3 tridomain harboring the V1314D amino acid substitution. The mechanism of quenching the A1 domain fluorescence has been previously shown to be collisional since the quenching constant is decreased at lower temperature (41), but we cannot exclude the possibility (albeit unlikely) that quenching in the V1314D A1A2A3 tridomain could be static, wherein a non-fluorescent complex is formed between tryptophans and acrylamide due to altered quaternary interactions between the A domains.

Furthermore, 8-anilino-1-naphthalenesulfonic acid (ANS) fluorescence spectra confirm the increased solvent exposure of the hydrophobic core of A1 due to the V1314D substitution showing an enhanced ANS fluorescence corresponding to an increased ANS dye interaction with exposed hydrophobic residues of the V1314D variant relative to WT A1A2A3.

Figure 2 shows the impact of the V1314D variant on the thermodynamic stability of VWF A1A2A3 using differential scanning calorimetry (DSC). The excess heat capacity of both WT and V1314D A1A2A3 shows multiple domain contributions to unfolding (46), and both variants unfold within the same temperature range, 50–70°C. Using a thermodynamic model for three domains (see Supplementary Data), both WT and V1314D A1A2A3 unfolding heat capacities were deconvoluted into three overlapping equilibrium transitions, one for each of the A domains. Overall, unfolding of V1314D A1A2A3 occurs with a significantly lower total enthalpy (area under the excess heat capacity trace), with the height of the first transition, corresponding to the unfolding of A1 and A2, decreasing to a level below that of the second transition, corresponding to the unfolding of A3. Although the T_m values do not change dramatically for individual domains, their enthalpy is substantially reduced in V1314D as compared to WT A1A2A3.

Our interpretation of this observation is that the deleterious effect of V1314D on the native structure of A1 substantially

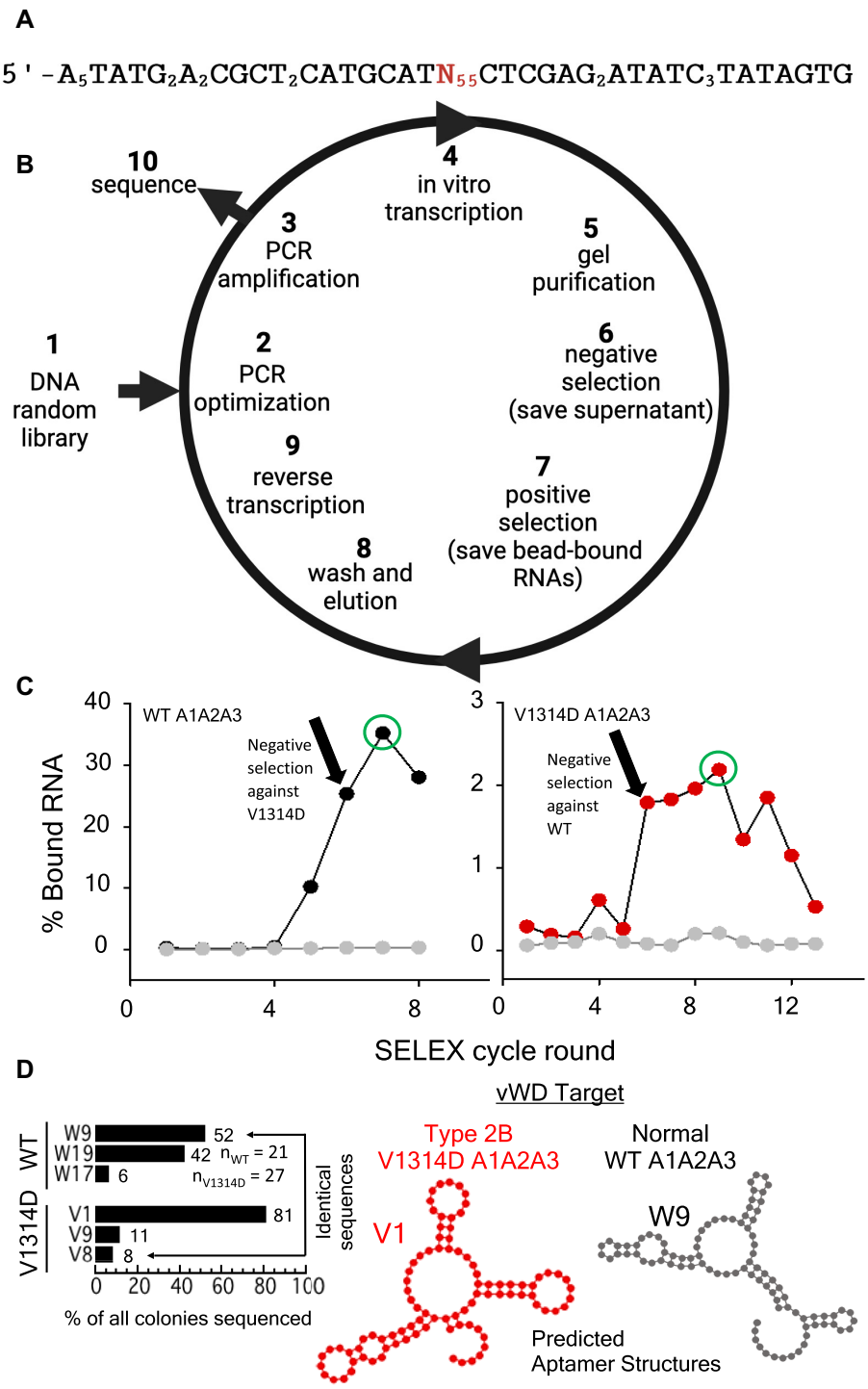

Figure 3. (**A**) Initial random DNA library to be transcribed for *in vitro* selection. 55-nucleotide random region (red) is flanked by forward and reverse primer binding sequences. (**B**) Experimental design to isolate and characterize nuclease-resistant RNA aptamers against VWFA1A2A3 variants. (1) Commercial single-stranded random DNA library. (2) Analytical PCR cycle optimization of random ssDNA library. (3) Preparative amplification of DNA library. (4) *In vitro* transcription of double-stranded DNA to 2′-fluoropyrimidine-containing RNA. (5) Gel purification of transcripts. (6) When indicated, negative selection against undesired immobilized target. (7) Positive selection against desired immobilized target. (8) Extensive washing and elution of target-bound RNAs. (9) Reverse transcription. The cycle then repeats at step 3. After the desired number of selections cycles (steps 2–9), a sample of library was analyzed by cloning and sequencing (step 10). (**C**) Percentages of RNA bound from the selections against WT (black symbols) and V1314D A1A2A3 (red symbols) are plotted as a function of selection cycle rounds. Green circled selection round material was used for aptamer cloning and sequencing. Negative controls (gray symbols) represent the percent bound RNA from selections against magnetic beads in the absence of proteins. Negative selection (arrow) was performed after six rounds of SELEX for each VWF variant against the other VWF variant. (**D**) Left: Prevalence of W9 and V1. Right: RNA secondary structures predicted by M-fold. Shown are the two most stable secondary structures of RNA aptamers selected against WT (W9) and V1314D A1A2A3 (V1) forms of VWF.

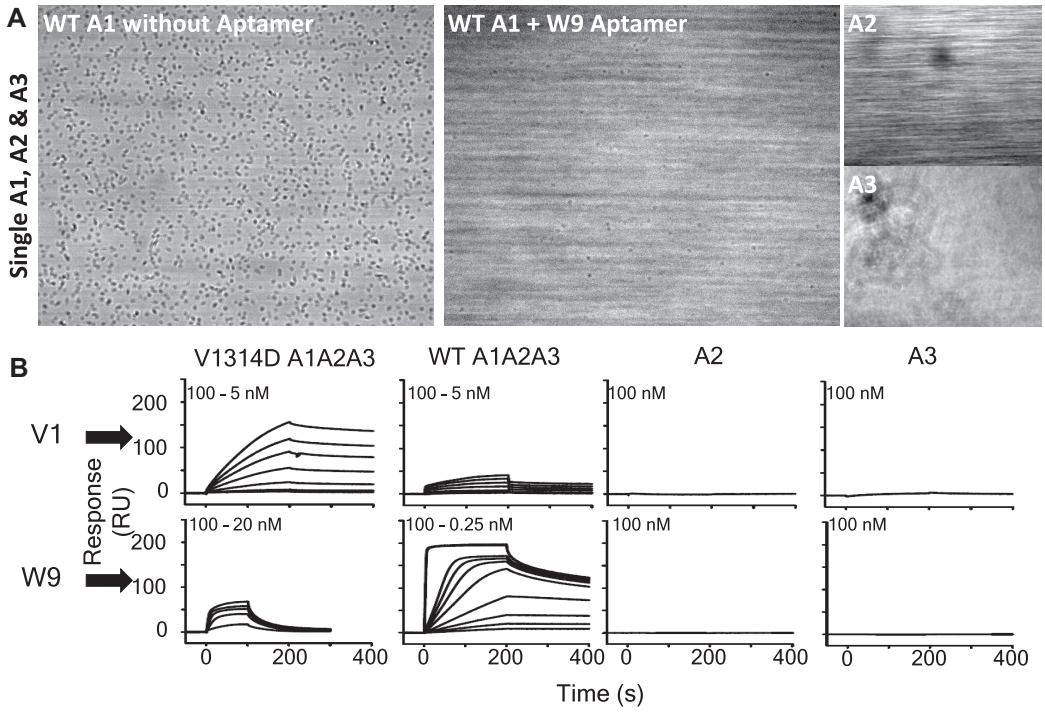

Figure 4. Domain specificity of W9 and V1. (**A**) Parallel plate shear flow assay at a shear rate of 800 s^{-1} with surface-immobilized single WT A1, in absence of or pre-treated with W9. Images on the right were taken with immobilized A2 and A3—both domains do not bind platelets. Approximate number of platelets per frame: WT A1 without W9: 1634 ±141; WT A1 with W9: 46 ±9. Platelet counts were estimated from four different images using Image Pro Premier 9.1 (Media Cybernetics). (**B**) Left: SPR experiments with WT and V1314D A1A2A3 to demonstrate specific binding of the aptamers to their target proteins. Experiments in right panels were performed to exclude the possibility that W9 and V1 recognize A2 and A3. W9 inhibits shear-induced binding of platelets to WT A1. Both Aptamers bind their target proteins but not A2 or A3. Thus, W9 and V1 specifically recognize native and misfolded A1 domains in the context of the A1A2A3 tri-domain.

reduces the overall unfolding cooperativity of A1. The mutation also affects the unfolding cooperativity of the neighboring A2 and A3 domains by disrupting native contact interactions between A1, A2 and A3. A recent study of the thermal unfolding of A1A2A3 with the A2 vicinal disulfide bond mutated to vicinal serines demonstrated domain uncoupling primarily through changes in T_m (46). With V1314D, we note primarily a loss of enthalpy, rather than changes in T_m, which suggests that new interactions between misfolded A1, A2 and A3 domains may occur, thereby substantially altering the overall conformation of A1A2A3 in an, as of yet, unpredictable manner.

Taken together, the spectroscopy (Figure 1) and DSC (Figure 2) results clearly confirm that WT A1A2A3 is significantly altered by the mutation such that V1314D A1A2A3 can be considered fundamentally different in both its conformation, structure, and thermodynamic properties. These substantial differences prompted the following experiments to isolate distinct RNA aptamers to distinguish the disease-delated phenotype from the normal phenotype, based upon the conformational consequences of a type 2B mutation in the A1 domain on the entire A1A2A3 region of VWF.

Targeting a misfolded A1 domain with RNA Aptamers through *in vitro* selection

Having confirmed variant-induced misfolding of A1 within the VWF tri-domain, we sought to use *in vitro* selection to identify RNA aptamers capable of specifically targeting native and disordered conformational states of the protein (Figure 3A). *In vitro* selection (Figure 3B) exploited a random RNA library including nuclease-resistant 2′-fluoropyrimidine nucleotides to identify specific ligands for purified WT versus V1314D variant A1A2A3 VWF tri-domains through multiple selection rounds. Each round conformed to the cycle shown in Figure 3B, ultimately resulting in an enrichment of aptamers that specifically bind WT versus variant V1314D forms of A1A2A3. Figure 3C shows the enrichment of aptamers as a function of selection cycle. After six cycles, a negative selection was performed to reduce aptamers with affinity for the non-targeted tri-domain. The left panel of Figure 3D shows the frequencies of aptamers W9, W19 and W17 (raised against WT A1A2A3) and V1, V9 and V8 (raised against V1314D A1A2A3) identified by cloning and Sangar sequencing after *in vitro* selection. Plausible RNA secondary structures were predicted using M-fold (e.g. V1 and W9 in Figure 3D). Because aptamers W9 and V1 showed the greatest abundance after sequencing, they were characterized in greater detail.

W9 and V1 specifically bind WT and V1314D variant A1A2A3, respectively

We expressed and purified the isolated WT A1 VWF domain in *E. coli* and immobilized it via an N-terminal His_6-tag on one channel of a Cu^{++}-chelated Cellix Vena8 Chip. Figure 4A shows images of platelets passing over the immobilized WT A1 domain at a shear rate of 800 s^{-1} in the absence or presence of supplemented W9. While platelet capture is normal in absence of W9, capture is substantially reduced in presence of W9. This observation is consistent with aptamer binding to

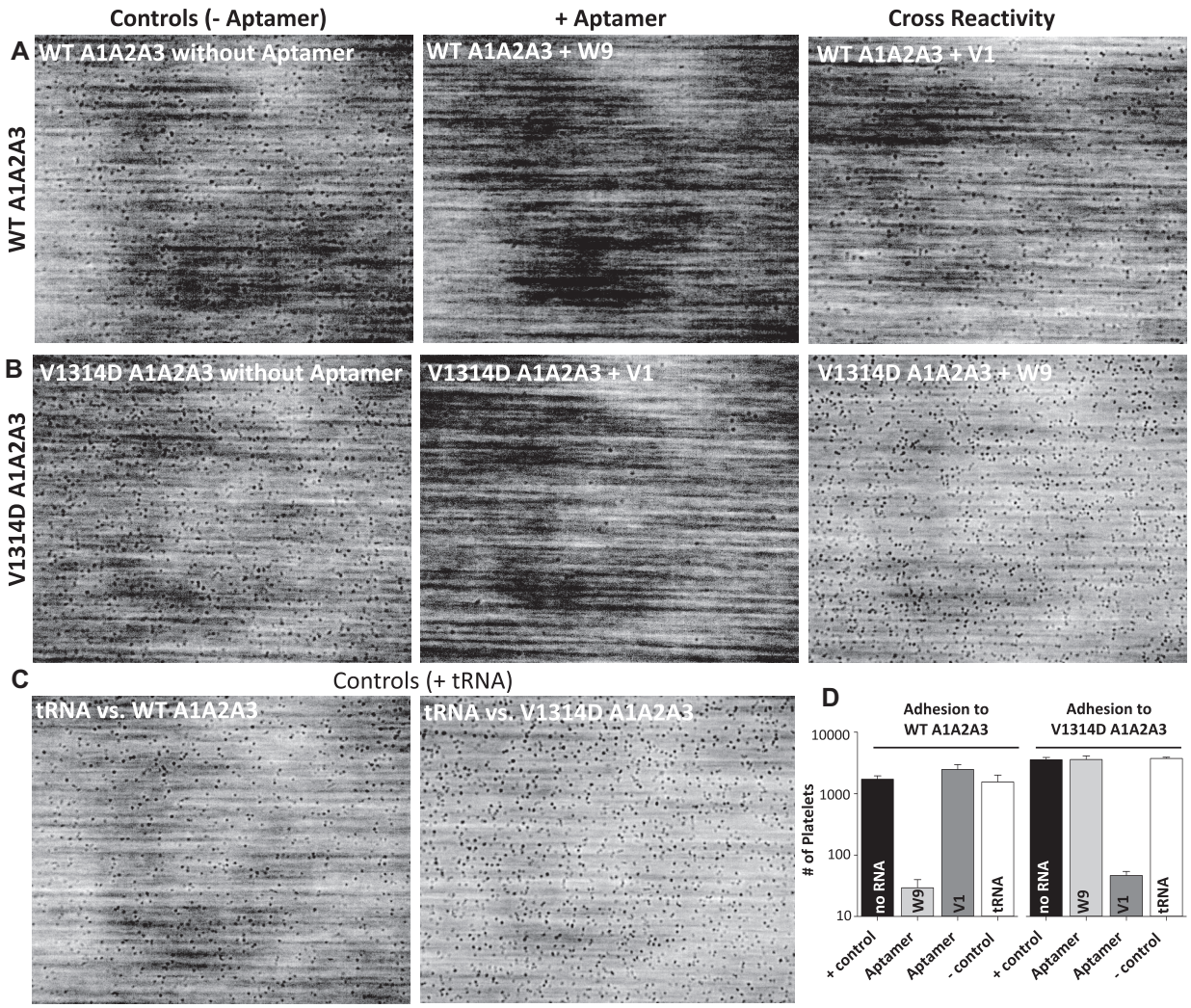

Figure 5. Aptamer inhibition of platelet adhesion to WT and V1314D A1A2A3 at a shear stress of 800 s^{-1}. (**A**) Adhesion of platelets to WT A1A2A3 in absence and presence of W9 and cross-reactivity with V1 (left to right). (**B**) Adhesion of platelets to V1314D A1A2A3 in absence of and presence of V1 and cross-reactivity with W9 (left to right). (**C**) Negative controls. No inhibition effect of transfer RNA on platelet adhesion to WT (left) and V1314D A1A2A3 (right). (**D**) Bar plot representation of specific inhibition of WT A1A2A3 and V1314D A1A2A3 by W9 and V1 aptamers. Reported platelet counts and error bars (standard deviation) were estimated from four different images using Image Pro Premier 9.1 (Media Cybernetics). The flow assay experiments demonstrate that W9 and V1 specifically inhibit the platelet binding function of their target proteins, WT and V1314D A1A2A3. All platelet counts above 1000 in panel (D) were not statistically different for either WT A1A2A3 (left) or V1314D A1A2A3 (right); *P*-value > 0.33 or 0.22, respectively. Platelet counts <100 for aptamer inhibition were statistically significant from platelet counts in the absence of either the W9 aptamer (left) or V1 aptamer (right); *P*-value $< 10^{-6}$.

A1 in a manner that competes with the interaction of A1 with platelet GPIbα. The A2 and A3 domains do not bind platelets under shear stress (see right images in Figure 4A). We utilized SPR experiments to evaluate the specificities of aptamers W9 and V1. Figure 4B shows that V1 and W9 preferentially bind to their target A1 domains while binding to A2 and A3 is negligible. The low cross-reactivity presumably reflects the conformational difference of A1 within A1A2A3.

Parallel plate shear flow assays were also performed with WT and V1314D variant A1A2A3 forms of VWF. Figure 5A shows images of platelets passing over surface-immobilized tri-domains under shear stress shortly after replacing the loaded whole citrated blood with Tris-buffered saline (TBS, 25 mM Tris-HCl, 150 mM NaCl, pH 7.4). This result demonstrates that aptamer W9 effectively inhibits the adherence of platelets to WT A1A2A3 while aptamer V1 has little effect. In turn, Figure 5B shows strong binding of platelets to the V1314D A1A2A3 tri-domain, while pre-treatment of the protein with aptamer V1 largely abolishes platelet binding. There is again little effect of W9 on the behavior of V1314D A1A2A3. Figure 5C confirms that inhibition is due to the specificity of the aptamers for their targets and this inhibition was not observed when proteins with were treated with transfer RNA. Panel D of Figure 5 shows an estimation of the number of platelets detected in the videos (provided as Supplementary Data).

We conclude that the platelet flow studies presented in Figures 4 and 5 establish W9 and V1 as specific reagents that selectively bind their targeted A1 domains with corresponding ability to inhibit platelet adherence. Low cross-reactivity confirms that WT and V1314D variant A1A2A3 tri-domains display distinctly different structures defined by these specific ap-

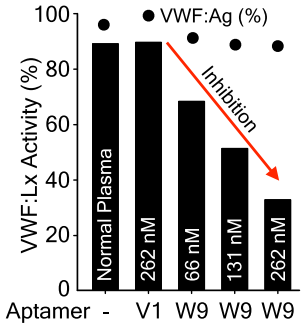

Figure 6. Aptamer inhibition of VWF:Lx activity. Bar plots represents VWF activity in the presence of W9 and V1 aptamers as determined by immuno-turbidity latex assay. Dots indicates the VWF antigen levels in NPP used in this study. Anti-VWF antibody-coated latex beads are pre-incubated with NPP in the presence of increasing concentrations (66, 131 and 262 nM) of W9 aptamer or V1 aptamer (262 nM). W9 inhibition of the VWF:Lx activity is dose dependent.

tamer reagents, consistent with the spectroscopic and calorimetric characterizations shown in Figures 1 and 2.

Aptamers W9 and V1 specifically bind targeted A1 forms in multimeric VWF

Having documented the interaction of W9 and V1 aptamers with their recombinant target VWF proteins and the resulting specific inhibition of platelet interactions, we sought to determine the performance of W9 and V1 in a clinical analytical setting.

To begin, we determined whether W9 could inhibit a clinical VWF activity assay employed at the Mayo Clinic Special Coagulation Laboratory. The VWF:Lx activity assay is an automated latex particle-enhanced immunoturbidometric VWF activity assay that has been validated through comparison with the VWF ristocetin cofactor activity (VWF:RCo) assay (49–51). Unlike the VWF:RCo assay, which has poor precision (52) and high interlaboratory variance (53,54), the VWF:Lx activity assay is reported to provide excellent diagnostic accuracy with high sensitivity and specificity for diagnosing severe VWD and acquired von Willebrand syndromes (49). Figure 6 demonstrates that the W9 aptamer reduces the VWF:Lx activity in a concentration-dependent manner between 0 and 262 nM final concentrations, indicating that W9 effectively competes against HemosIL for binding the VWF A1 domain and thus prevents agglutination of the monoclonal antibody conjugated latex particles (55,56).

We then studied the binding of both aptamers to commercial, enriched and dialyzed Wilate VWF/factor VIII concentrate. SPR experiments were performed with streptavidin immobilized, biotinylated aptamer W9 (Figure 7A), demonstrating that the aptamer tightly interacts with native A1 domains in the supplied VWF Wilate. In contrast (and in agreement with the A1A2A3 flow assay and SPR data shown in Figures 4 and 5), aptamer V1 did not interact with the supplied Wilate. As a next test, we loaded NPP (provided by the Mayo Clinic Special Coagulation Laboratory) onto surface-immobilized aptamers (Figure 7B). Again, aptamer W9 was observed to tightly interact with the VWF supplied in human plasma, while V1 did not. In a final SPR experiment, we studied the interaction between the aptamers and a 2B patient sample (also provided by Mayo Clinic Special Coagulation Laboratory). This donor carries R1306W (57) as a heterozygous variant affecting the A1 domain of VWF. The sample therefore contained a mixture of R1306W and normal plasma VWF. Figure 7C confirms the presence of both normal and pathological A1 variant domains in the patient sample, as both aptamers were able to bind.

The SPR experiments shown in Figure 7 confirm that W9 and V1 aptamers specifically bind the corresponding normal and abnormal conformations of the A1 domain in the context of multimeric VWF supplied either as purified VWF (Wilate), in normal plasma, or in heterozygous 2B patient plasma. The ability of the V1 aptamer to detect A1 disorder due to the R1306W variant suggests that the altered conformations of V1314D and R1306W reveal a common 2B VWD conformational property detected by this reagent.

W9 and V1 specifically inhibit ristocetin-induced platelet agglutination

Ristocetin-induced platelet agglutination (RIPA) is widely used as a clinical test to diagnose type 2B VWD and platelet-type VWD, in which the platelet receptor GPIbα is hyperactive due to gain of function mutations. We utilized RIPA to the determine whether aptamers W9 and V1 inhibit the formation of VWF-mediated platelet aggregates.

Figure 8 shows the platelet agglutination in presence of 0.5 or 0.375 mg/ml ristocetin for normal plasma and R1306W heterozygous patient plasma, respectively. In the absence of aptamer, platelets quickly aggregated with plasma VWF under the influence of the supplied ristocetin, as expected. Addition of 5, 10 or 100 nM aptamer W9 resulted in delayed agglutination, indicating that W9 inhibits the RIPA assay. In contrast, addition of 100 nM V1 to normal plasma only marginally inhibited platelet agglutination and a mixture of 100 nM V1 and 100 nM W9 resulted in agglutination kinetics identical to those of W9 alone. These results demonstrate that V1 does not inhibit RIPA of normal plasma, consistent with prior results obtained for VWF:Lx activity, A1A2A3, Wilate and NPP forms of VWF in flow assays and SPR experiments. The right panel of Figure 8 presents the results of RIPA for plasma from the heterozygous R1306W type 2B VWD patient. Here W9 and V1 show similar inhibitory effects on platelet agglutination, while their combination is effective in blocking platelet agglutination. These RIPA experiments demonstrate that both selected aptamers detect and inhibit the activities of normal and abnormal A1 with high specificity.

Discussion

Disordered VWD conformations of the A1 domain most certainly alter the binding specificity of GPIbα and can alter the epitopes for molecular probes targeting VWF. Instead of viewing conformational disorder as a detriment to assay design, we have used the SELEX platform to isolate two aptamers that discriminate normal from disease states in A1A2A3. The results of this study confirm that the resulting 2′-fluoro pyrimidine RNA aptamers, W9 and V1, bind and inhibit platelet interactions with their specific targets with minimal cross-reactivity in equilibrium SPR assays, clinical assays utilizing plasma VWF, and platelet adhesion under the shear stress of blood flow. This study establishes the principle of sensitive disorder recognition by RNA analog aptamers that effectively detect pathological conformations of VWF.

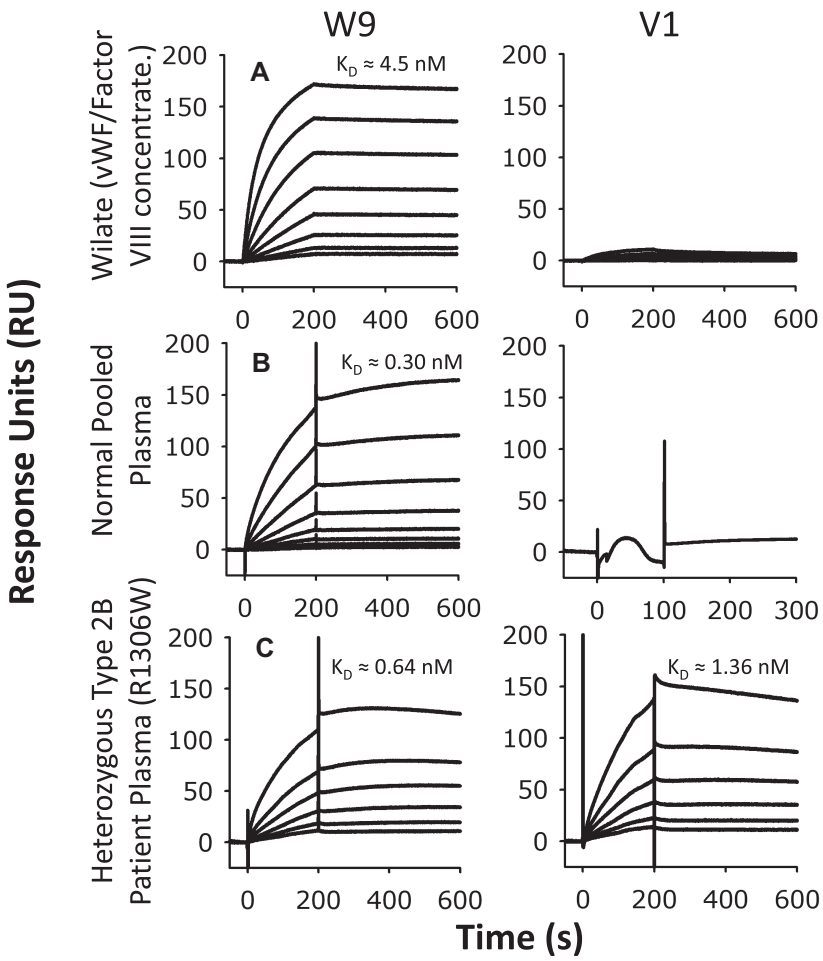

Figure 7. SPR-interaction of neutravidin-captured biotinylated W9 and V1 with Wilate (VWF/Factor VIII concentrate) (**A**), diluted NPP (**B**) and diluted heterozygous type 2B VWD (R1306W) patient plasma (**C**). W9 recognizes native A1 domains in all three samples, while V1 selectively recognizes partially disordered states of A1 harboring the R1306W variant (57). Nanomolar K_D-value estimates were obtained assuming 1:1 binding.

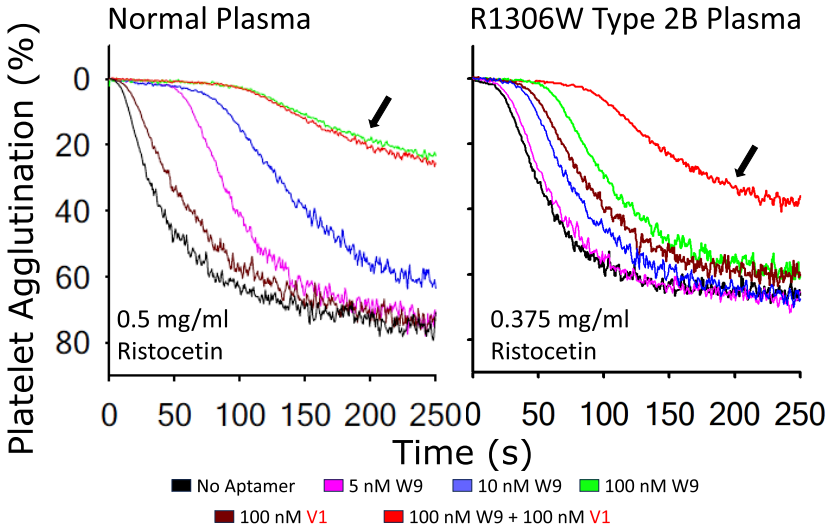

Figure 8. Aptamer-induced inhibition of RIPA of normal pool plasma (left) and heterozygous R1306W Type 2B patient plasma (right). In normal plasma, platelet agglutination is efficiently inhibited by W9 in a dose-dependent manner while the addition of 100 nM V1 alone or in combination with W9 (arrow) has little effect. In the heterozygous R1306W type 2B patient plasma, 100 nM W9 or V1 have similar small inhibitory effects, while their combination shows clear RIPA inhibition (arrow). Taken together these results demonstrate that W9 and V1 can recognize native and disordered A1 domains in plasma.

The discrimination that W9 and V1 provide for plasma VWF from a VWD patient compared to normal VWF is strong evidence that the conformational properties of A1A2A3 altered by the mutation are similar, if not identical, to those within full length multimeric VWF in plasma. A1A2A3 is the largest fragment of VWF employed to date to elicit aptamers that block A1 domain platelet function. As a result, A1A2A3 provides an ideal substrate for aptamer recognition because it retains quaternary interactions with the neighboring A2 and A3 domains (46) and the O-glycosylation present in the N-terminal A1 flanking sequence and the A1A2 linker sequence (58–62), together with the N-glycosylation present in A2 (6,63). This is a significant benefit for aptamer design as it accounts for all the secondary, tertiary and quaternary properties of the VWF A domains that regulate VWF function in primary hemostasis.

Prior aptamers, rondoraptivon pegol and ARC1779, target only WT A1 (20,35). Although clinical trials with a type 2B patient showed improvements in platelet counts, VWF antigen levels, FVIII activity, ristocetin cofactor activity, activated partial thromboplastin time, restoration of high molecular weight multimers of VWF, and inhibition of desmopressin aggravated thrombocytopenia (17,21,27,28), it could be argued that these improvements could be primarily due to aptamer inhibition of normally structured A1 domains within plasma VWF multimers, not the result of specific targeting of VWD variant A1 domains. VWD is a phenotypically heterogeneous bleeding disorder (64). A complicating factor in the most recent type 2B clinical trial (17) was that the patients maintained their regular infusion of recombinant VWF during treatment with the aptamer. The authors acknowledge that rondoraptivon pegol binds WT VWF and this likely influences the clinically measured VWF parameters. They also acknowledge that mutations could alter the structure of VWF and thus compromise the binding of the aptamer to the afflicted A1 domains.

In fact, the variants described in this trial (17), R1306W, R1308C, W1313C and V1316M, are likely disordered. V1316M is certainly disordered (38,40) and is as phenotypically severe as V1314D with substantially enhanced platelet translocation pause times on surface immobilized A1 under shear flow and severe thrombocytopenia in patients. Platelet translocation pause times under shear flow across surface immobilized A1 domains and thrombocytopenia in VWD patients were found to be directly correlated, $R^2 = 0.88$ (40). Both of these variants occur in the β2 strand of A1, and while V1314D introduces a negative charge, V1316M introduces a larger methionine side chain resulting in steric hinderances in the hydrophobic core of the domain that locally destabilize the α2 helix (40).

R1306W likely has similar effects on the α1-loop-β2 and α2-helical regions and while we have not directly studied R1306W, we have shown that the type 2B R1306Q variant is thermodynamically destabilized due to loss of a salt bridge with D1451 in α6 putting it on pathway to local disorder in the region (40). Recognition of R1306W plasma VWF by the V1 aptamer, which was selected against V1314D, indicates that the structural changes or the enhanced dynamics caused by R1306W are similar to V1314D. Therefore, we expect that the dynamic nature and the propensity of these α1-loop-β2 and α2-helical regions to locally unfold are a common trait of type 2B VWD.

Many of the type 2M VWD variants are also disordered (40), though likely in different regions of the A1 domain structure than that for type 2B (43). The principle of disorder recognition established here for type 2B could also be applied to type 2M VWD, wherein aptamers selected against misfolded loss-of-function states could be applied to VWD diagnostics. The utility of an anti-2M aptamer in this manner may not be an ideal therapeutic and variants that hyperstabilize the A1 domain native structure (44) may be refractory to such a conformationally sensitive aptamer that targets disorder in the loss-of-function phenotype.

This study provides strong evidence that VWF disease states can be targeted specifically based on their intrinsic conformational differences. Although the pharmocokinetic properties of W9 and V1 have not yet been determined, PEGylation has not been utilized, and bioactive regions of the 55 variable nucleotide sequences have not yet been identified, W9 and V1 are intrinsically nuclease resistant owing to their 2′-fluorinated pyrimidine modifications. This property of these aptamers should confer *in vitro* stability for laboratory diagnostics and could also be beneficial to their stability as therapeutics for type 2B VWD *in vivo*.

Our prior studies have established structural disorder as a hallmark of type 2 VWD. This study establishes aptamers as powerful tools for the detection and recognition of structurally disordered conformations that contribute to disease phenotypes. It is expected that the principles demonstrated here could also benefit diagnosis and therapeutic interventions involving other protein folding disorders.

Data availability

Plasmids for protein expression are available upon request. Aptamer sequences have been disclosed to Mayo Clinic Ventures and can be shared upon request.

Supplementary data

Supplementary Data are available at NARMME Online.

Acknowledgements

The authors acknowledge members of the Auton and Maher Laboratories and Mayo Clinic Special Coagulation Laboratory for technical assistance.

Author contributions: Protein Expression and purification: L.M.T., V.R.M. and A.T. Protein quality control, spectroscopy and unfolding experiments: A.T. and V.R.M. SELEX: V.R.M. and A.S.D. Parallel Plate Flow Assay: V.R.M., A.T. and M.A. SPR experiments: V.R.M. Experimental design: V.R.M., A.T., L.J.M. and M.A. Manuscript preparation: V.R.M., A.T., L.J.M. and M.A.

Funding

National Heart, Lung, and Blood Institute [HL146508 to M.A.]; Great Lakes Hemophilia Foundation and Health Resources and Services Administration through the Mayo Clinic Comprehensive Hemophilia Treatment Center [H30MC24052 to M.A. and R.K.P.]; National Institute of General Medical Sciences [GM143949 to L.J.M., III].

Conflict of interest statement

None declared.

References

1. Fu,H., Jiang,Y., Yang,D., Scheiflinger,F., Wong,W. and Springer,T. (2017) Flow-induced elongation of von Willebrand factor precedes tension-dependent activation. *Nat. Commun.*, **8**, 324.
2. Terraube,V., O'Donnell,J. and Jenkins,P. (2010) Factor VIII and von Willebrand factor interaction: biological, clinical and therapeutic importance. *Haemophilia*, **16**, 3–13.
3. Sadler,J., Budde,U., Eikenboom,J., Favaloro,E., Hill,F., Holmberg,L., Ingerslev,J., Lee,C., Lillicrap,D., Mannucci,P., *et al.* (2006) Update on the pathophysiology and classification of von Willebrand disease: a report of the Subcommittee on von Willebrand factor. *J. Thromb. Haemost.*, **4**, 2103–2114.
4. Berber,E. (2012) The molecular genetics of von Willebrand disease. *Turk. J. Haematol.*, **29**, 313–324.
5. Keeney,S. and Cumming,A. (2001) The molecular biology of von Willebrand disease. *Clin. Lab. Haematol.*, **23**, 209–230.
6. Lynch,C. and Lane,D. (2016) N-linked glycan stabilization of the VWF A2 domain. *Blood*, **127**, 1711–1718.
7. Lynch,C., Cawte,A., Millar,C., Rueda,D. and Lane,D. (2017) A common mechanism by which type 2A von Willebrand disease mutations enhance ADAMTS13 proteolysis revealed with a von Willebrand factor A2 domain FRET construct. *PLoS One*, **12**, e0188405.
8. Castaman,G., Federici,A., Tosetto,A., La Marca,S., Stufano,F., Mannucci,P. and Rodeghiero,F. (2012) Different bleeding risk in type 2A and 2M von Willebrand disease: a 2-year prospective study in 107 patients. *J. Thromb. Haemost.*, **10**, 632–638.
9. Favaloro,E., Bonar,R. and Marsden,K. (2012) Different bleeding risk in type 2A and 2M von Willebrand disease: a 2-year prospective study in 107 patients: a rebuttal. *J. Thromb. Haemost.*, **10**, 1455–1458.
10. Hulstein,J., de Groot,P., Silence,K., Veyradier,A., Fijnheer,R. and Lenting,P. (2005) A novel nanobody that detects the gain-of-function phenotype of von Willebrand factor in ADAMTS13 deficiency and von Willebrand disease type 2B. *Blood*, **106**, 3035–3042.
11. Federici,A., Mannucci,P., Castaman,G., Baronciani,L., Bucciarelli,P., Canciani,M., Pecci,A., Lenting,P. and De Groot,P. (2009) Clinical and molecular predictors of thrombocytopenia and risk of bleeding in patients with von Willebrand disease type 2B: a cohort study of 67 patients. *Blood*, **113**, 526–534.
12. Chen,J., Hinckley,J., Haberichter,S., Jacobi,P., Montgomery,R., Flood,V., Wong,R., Interlandi,G., Chung,D., López,J., *et al.* (2015) Variable content of von Willebrand factor mutant monomer drives the phenotypic variability in a family with von Willebrand disease. *Blood*, **126**, 262–269.
13. Ulrichts,H., Silence,K., Schoolmeester,A., de Jaegere,P., Rossenu,S., Roodt,J., Priem,S., Lauwereys,M., Casteels,P., Van Bockstaele,F., *et al.* (2011) Antithrombotic drug candidate ALX-0081 shows superior preclinical efficacy and safety compared with currently marketed antiplatelet drugs. *Blood*, **118**, 757–765.
14. Peyvandi,F. and Duby,C. (2014) Caplacizumab, anti-VWF nanobody potentially changing the treatment paradigm in thrombotic thrombocytopenic purpura: results of the TITAN trial. *Blood*, **124**, 229.
15. Peyvandi,F., Scully,M., Kremer Hovinga,J., Knöbl,P., Cataland,S., De Beuf,K., Callewaert,F., De Winter,H. and Zeldin,R. (2017) Caplacizumab reduces the frequency of major thromboembolic events, exacerbations and death in patients with acquired thrombotic thrombocytopenic purpura. *J. Thromb. Haemost.*, **15**, 1448–1452.
16. Ay,C., Kovacevic,K.D., Kraemmer,D., Schoergenhofer,C., Gelbenegger,G., Firbas,C., Quehenberger,P., Jilma-Stohlawetz,P., Gilbert,J.C., Zhu,S., *et al.* (2023) The von Willebrand factor–binding aptamer rondaptivon pegol as a treatment for severe and nonsevere hemophilia A. *Blood*, **141**, 1147–1158.
17. Ay,C., Pabinger,I., Kovacevic,K., Gelbenegger,G., Schörgenhofer,C., Quehenberger,P., Jilma-Stohlawetz,P., Sunder-Plassman,R., Gilbert,J., Zhu,S., *et al.* (2022) The VWF binding aptamer rondoraptivon pegol increases platelet counts and VWF/FVIII in type 2B von Willebrand disease. *Blood Adv*, **6**, 5467–5476.
18. Kim,M., Hajducek,D., Gilbert,J., Iorio,A., Jilma,B. and Edginton,A. (2024) Kinetic modeling for BT200 to predict the level of plasma-derived coagulation factor VIII in humans. *AAPS J*, **26**, 81.
19. Chan Kwo Chion,A., Byrne,C., Atiq,F., Doherty,D., Aguila,S., Fazavana,J., Lopes,P., Karampini,E., Amin,A., Preston,R., *et al.* (2024) Aptamer BT200 blocks interaction of K1405-1408 in the VWF-A1 domain with macrophage LRP1. *Blood*, **144**, 1445-1456.
20. Zhu,S., Gilbert,J., Hatala,P., Harvey,W., Liang,Z., Gao,S., Kang,D. and Jilma,B. (2020) The development and characterization of a long acting anti-thrombotic von Willebrand factor (VWF) aptamer. *J. Thromb. Haemost.*, **18**, 1113–1123.
21. Kovacevic,K., Grafeneder,J., Schörgenhofer,C., Gelbenegger,G., Gager,G., Firbas,C., Quehenberger,P., Jilma-Stohlawetz,P., Bileck,A., Zhu,S., *et al.* (2022) The von Willebrand factor A-1 domain binding aptamer BT200 elevates plasma levels of von Willebrand factor and factor VIII: a first-in-human trial. *Haematologica*, **107**, 2121–2132.
22. Kovacevic,K., Buchtele,N., Schoergenhofer,C., Derhaschnig,U., Gelbenegger,G., Brostjan,C., Zhu,S., Gilbert,J. and Jilma,B. (2020) The aptamer BT200 effectively inhibits von Willebrand factor (VWF) dependent platelet function after stimulated VWF release by desmopressin or endotoxin. *Sci. Rep.*, **10**, 11180.
23. Siller-Matula,J., Merhi,Y., Tanguay,J., Duerschmied,D., Wagner,D., McGinness,K., Pendergrast,P., Chung,J., Tian,X., Schaub,R. and et,al. (2012) ARC15105 is a potent antagonist of von Willebrand factor mediated platelet activation and adhesion. *Arterioscler. Thromb. Vasc. Biol.*, **32**, 902–909.
24. Chen,W., Voos,K., Josephson,C. and Li,R. (2019) Short-acting anti-VWF (von Willebrand factor) aptamer improves the recovery, survival, and hemostatic functions of refrigerated platelets. *Arterioscler. Thromb. Vasc. Biol.*, **39**, 2028–2037.
25. Gilbert,J., DeFeo-Fraulini,T., Hutabarat,R., Horvath,C., Merlino,P., Marsh,H., Healy,J., Boufakhreddine,S., Holohan,T. and Schaub,R. (2007) First-in-human evaluation of anti von Willebrand factor therapeutic aptamer ARC1779 in healthy volunteers. *Circulation*, **116**, 2678–2686.
26. Diener,J., Daniel Lagassé,H., Duerschmied,D., Merhi,Y., Tanguay,J., Hutabarat,R., Gilbert,J., Wagner,D. and Schaub,R. (2009) Inhibition of von Willebrand factor-mediated platelet activation and thrombosis by the anti-von Willebrand factor A1-domain aptamer ARC1779. *J. Thromb. Haemost.*, **7**, 1155–1162.
27. Jilma,B., Paulinska,P., Jilma-Stohlawetz,P., Gilbert,J., Hutabarat,R. and Knöbl,P. (2010) A randomised pilot trial of the anti-von Willebrand factor aptamer ARC1779 in patients with type 2b von Willebrand disease. *Thromb. Haemost.*, **104**, 563–570.
28. Jilma-Stohlawetz,P., Knöbl,P., Gilbert,J. and Jilma,B. (2012) The anti-von Willebrand factor aptamer ARC1779 increases von Willebrand factor levels and platelet counts in patients with type 2B von Willebrand disease. *Thromb. Haemost.*, **108**, 284–290.
29. Knöbl,P., Jilma,B., Gilbert,J., Hutabarat,R., Wagner,P. and Jilma-Stohlawetz,P. (2009) Anti-von Willebrand factor aptamer ARC1779 for refractory thrombotic thrombocytopenic purpura. *Transfusion*, **49**, 2181–2185.
30. Mayr,F., Knöbl,P., Jilma,B., Siller-Matula,J., Wagner,P., Schaub,R., Gilbert,J. and Jilma-Stohlawetz,P. (2010) The aptamer ARC1779 blocks von Willebrand factor-dependent platelet function in patients with thrombotic thrombocytopenic purpura *ex vivo*. *Transfusion*, **50**, 1079–1087.
31. Jilma-Stohlawetz,P., Gilbert,J., Gorczyca,M., Knöbl,P. and Jilma,B. (2011) A dose ranging phase I/II trial of the von Willebrand factor inhibiting aptamer ARC1779 in patients with congenital thrombotic thrombocytopenic purpura. *Thromb. Haemost.*, **106**, 539–547.
32. Jilma-Stohlawetz,P., Gorczyca,M., Jilma,B., Siller-Matula,J., Gilbert,J. and Knöbl,P. (2011) Inhibition of von Willebrand factor by ARC1779 in patients with acute thrombotic thrombocytopenic purpura. *Thromb. Haemost.*, **105**, 545–552.

33. Sakai,K., Someya,T., Harada,K., Yagi,H., Matsui,T. and Matsumoto,M. (2020) Novel aptamer to von Willebrand factor A1 domain (TAGX-0004) shows total inhibition of thrombus formation superior to ARC1779 and comparable to caplacizumab. *Haematologica*, **105**, 2631–2638.
34. Spiel,A., Mayr,F., Ladani,N., Wagner,P., Schaub,R., Gilbert,J. and Jilma,B. (2009) The aptamer ARC1779 is a potent and specific inhibitor of von Willebrand Factor mediated *ex vivo* platelet function in acute myocardial infarction. *Platelets*, **20**, 334–340.
35. Huang,R., Fremont,D., Diener,J., Schaub,R. and Sadler,J. (2009) A structural explanation for the antithrombotic activity of ARC1172, a DNA aptamer that binds von Willebrand factor domain A1. *Structure*, **17**, 1476–1484.
36. Vaganov,A., Taranushenko,T., Luzan,N., Shchugoreva,I., Kolovskaya,O., Artyushenko,P., Zamay,T. and Kichkailo,A. (2022) Aptamers regulating the hemostasis system. *Molecules*, **27**, 8593.
37. Nimjee,S., Dornbos,D., Pitoc,G., Wheeler,D., Layzer,J., Venetos,N., Huttinger,A., Talentino,S., Musgrave,N., Moody,H., *et al.* (2019) Preclinical development of a vWF aptamer to limit thrombosis and engender arterial recanalization of occluded vessels. *Mol. Ther.*, **27**, 1228–1241.
38. Tischer,A., Brehm,M., Machha,V., Moon-Tasson,L., Benson,L., Nelton,K., Leger,R., Obser,T., Martinez-Vargas,M., Whitten,S., *et al.* (2020) Evidence for the misfolding of the A1 domain within multimeric von Willebrand factor in Type 2 von Willebrand disease. *J. Mol. Biol.*, **432**, 305–323.
39. Tischer,A., Machha,V., Frontroth,J., Brehm,M., Obser,T., Schneppenheim,R., Mayne,L., Walter Englander,S. and Auton,M. (2017) Enhanced local disorder in a clinically elusive von Willebrand factor provokes high-affinity platelet clumping. *J. Mol. Biol.*, **429**, 2161–2177.
40. Tischer,A., Madde,P., Moon-Tasson,L. and Auton,M. (2014) Misfolding of vWF to pathologically disordered conformations impacts the severity of von Willebrand disease. *Biophys. J.*, **107**, 1185–1195.
41. Tischer,A., Madde,P., Blancas-Mejia,L. and Auton,M. (2014) A molten globule intermediate of the von Willebrand factor A1 domain firmly tethers platelets under shear flow. *Proteins*, **82**, 867–878.
42. Auton,M., Zhu,C. and Cruz,M. (2010) The mechanism of VWF-mediated platelet GPIbalpha binding. *Biophys. J.*, **99**, 1192–1201.
43. Zimmermann,M., Tischer,A., Whitten,S. and Auton,M. (2015) Structural origins of misfolding propensity in the platelet adhesive von Willebrand factor A1 domain. *Biophys. J.*, **109**, 398–406.
44. Tischer,A., Campbell,J., Machha,V., Moon-Tasson,L., Benson,L., Sankaran,B., Kim,C. and Auton,M. (2016) Mutational constraints on local unfolding inhibit the rheological adaptation of von Willebrand factor. *J. Biol. Chem.*, **291**, 3848–3859.
45. Casaña,P., Martínez,F., Haya,S., Tavares,A. and Aznar,J. (2001) New mutations in exon 28 of the von Willebrand factor gene detected in patients with different types of von Willebrand's disease. *Haematologica*, **86**, 414–419.
46. Tischer,A., Moon-Tasson,L. and Auton,M. (2023) Removal of the vicinal disulfide enhances the platelet capturing function of von Willebrand factor. *Blood*, **141**, 1469–1473.
47. Tischer,A., Machha,V., Rösgen,J. and Auton,M. (2018) 'Cooperative collapse' of the denatured state revealed through Clausius-Clapeyron analysis of protein denaturation phase diagrams. *Biopolymers*, **109**, e23106.
48. Campbell,J., Tischer,A., Machha,V., Moon-Tasson,L., Sankaran,B., Kim,C. and Auton,M. (2016) Data on the purification and crystallization of the loss-of-function von Willebrand disease variant (p.Gly1324Ser) of the von Willebrand factor A1 domain. *Data Brief*, **7**, 1700–1706.
49. Chen,D., Tange,J., Meyers,B., Pruthi,R., Nichols,W. and Heit,J. (2011) Validation of an automated latex particle-enhanced immunoturbidimetric von Willebrand factor activity assay. *J. Thromb. Haemost.*, **9**, 1993–2002.
50. de Maistre,E., Volot,F., Mourey,G., Aho,L., Ternisien,C., Briquel,M., Bertrand,M., Tardy,B., Frotscher,B., Nguyen,P., *et al.* (2014) Performance of two new automated assays for measuring von Willebrand activity: HemosIL AcuStar and Innovance. *Thromb. Haemost.*, **112**, 825–830.
51. Graf,L., Moffat,K., Carlino,S., Chan,A., Iorio,A., Giulivi,A. and Hayward,C. (2014) Evaluation of an automated method for measuring von Willebrand factor activity in clinical samples without ristocetin. *Int. J. Lab. Hematol.*, **36**, 341–351.
52. Meijer,P. and Haverkate,F. (2006) An external quality assessment program for von Willebrand factor laboratory analysis: an overview from the European concerted action on thrombosis and disabilities foundation. *Semin. Thromb. Hemost.*, **32**, 485–491.
53. Kitchen,S., Jennings,I., Woods,T., Kitchen,D., Walker,I. and Preston,F. (2006) Laboratory tests for measurement of von Willebrand factor show poor agreement among different centers: results from the United Kingdom National External Quality Assessment Scheme for Blood Coagulation. *Semin. Thromb. Hemost.*, **32**, 492–498.
54. Favaloro,E. (2011) Diagnosis and classification of von Willebrand disease: a review of the differential utility of various functional von Willebrand factor assays. *Blood Coagul Fibrinolysis*, **22**, 553–564.
55. Murdock,P., Woodhams,B., Matthews,K., Pasi,K. and Goodall,A. (1997) von Willebrand factor activity detected in a monoclonal antibody-based ELISA: an alternative to the ristocetin cofactor platelet agglutination assay for diagnostic use. *Thromb. Haemost.*, **78**, 1272–1277.
56. Chand,S., McCraw,A., Hutton,R., Tuddenham,E. and Goodall,A. (1986) A two-site, monoclonal antibody-based immunoassay for von Willebrand factor–demonstration that vWF function resides in a conformational epitope. *Thromb. Haemost.*, **55**, 318–324.
57. Ozeki,M., Kunishima,S., Kasahara,K., Funato,M., Teramoto,T., Kaneko,H., Fukao,T. and Kondo,N. (2010) A family having type 2B von Willebrand disease with an R1306W mutation: Severe thrombocytopenia leads to the normalization of high molecular weight multimers. *Thromb. Res.*, **125**, e17–e22.
58. Bonazza,K., Iacob,R., Hudson,N., Li,J., Lu,C., Engen,J. and Springer,T. (2022) Von Willebrand factor A1 domain stability and affinity for GPIba are differentially regulated by its O-glycosylated N- and C-linker. *Elife*, **11**, e75760.
59. Tischer,A., Machha,V., Moon-Tasson,L., Benson,L. and Auton,M. (2019) Glycosylation sterically inhibits platelet adhesion to von Willebrand factor without altering intrinsic conformational dynamics. *J. Thromb. Haemost.*, **18**, 79–90.
60. Schulte am Esch,J., Robson,S., Knoefel,W., Eisenberger,C., Peiper,M. and Rogiers,X. (2005) Impact of O-linked glycosylation of the VWF-A1-domain flanking regions on platelet interaction. *Br. J. Haematol.*, **128**, 82–90.
61. Nowak,A., Canis,K., Riddell,A., Laffan,M. and McKinnon,T. (2012) O-linked glycosylation of von Willebrand factor modulates the interaction with platelet receptor glycoprotein Ib under static and shear stress conditions. *Blood*, **120**, 214–222.
62. Canis,K., McKinnon,T., Nowak,A., Panico,M., Morris,H., Laffan,M. and Dell,A. (2010) The plasma von Willebrand factor O-glycome comprises a surprising variety of structures including ABH antigens and disialosyl motifs. *J. Thromb. Haemost.*, **8**, 137–145.
63. McKinnon,T., Chion,A., Millington,A., Lane,D. and Laffan,M. (2008) N-linked glycosylation of VWF modulates its interaction with ADAMTS13. *Blood*, **111**, 3042–3049.
64. Rendal,E., Penas,N., Larrabeiti,B., Pérez,A., Vale,A., López-Fernández,M. and Batlle,J. (2001) Type 2B von Willebrand's disease due to Val1316Met mutation. Heterogeneity in the same sibship. *Ann. Hematol.*, **80**, 354–360.

Received: October 10, 2024. **Revised:** November 14, 2024. **Editorial Decision:** November 19, 2024. **Accepted:** November 22, 2024